



NORAD Tracking of the 2022 February Starlink Satellites and the Immediate Loss of 32 Satellites

Fernando L. Guarnieri¹, Bruce T. Tsurutani², Rajkumar Hajra³, Ezequiel Echer⁴, Gurbax S. Lakhina⁵

5

¹Rua Serra das Vertentes, 56, São José dos Campos, São Paulo, Brazil. (ORCID 0009-0007-2353-2594)

²Retired, Pasadena, California USA. (ORCID 0000-0001-7299-9835)

³CAS Key Laboratory of Geospace Environment, School of Earth and Space Sciences, University of Science and Technology of China, Hefei, China. (ORCID 0000-0003-0447-1531)

10 ⁴Instituto Nacional de Pesquisas Espaciais, São José dos Campos, São Paulo, Brazil. (ORCID 0000-0002-8351-6779)

⁵Vashi, Navi Mumbai 400703, India. (ORCID 0000-0002-8956-486X)

Correspondence to: Fernando L. Guarnieri (fernando.guarnieri@gmail.com)

Abstract. The North American Aerospace Defense Command (NORAD) tracking of the SpaceX Starlink satellite launch on 2022 February 3 is reviewed. Of the 49 Starlink satellites released into orbit, 38 were eventually lost. Thirty-two of the satellites
15 were never tracked by NORAD. Two different physical mechanisms have been proposed published in Space Weather and one in arXiv to explain the satellite losses. It is argued that none of these three papers can explain the immediate loss of 32 of the 49 satellites. We suggest NORAD satellite tracking information for scientists to further investigate possible loss mechanisms.

1 Introduction

Geomagnetic storms (von Humboldt 1808; Gonzalez et al. 1994) are caused by magnetic reconnection (Dungey 1961;
20 Tsurutani and Meng, 1972; Paschmann et al., 1979) between southward interplanetary magnetic fields (IMFs) and the Earth's dayside magnetic fields. The reconnected magnetic fields and solar wind plasma are convected to the midnight sector of the Earth's magnetosphere (magnetotail) where the magnetic fields are reconnected again (Dungey, 1961). The reconnected fields and plasma are jetted from the magnetotail towards the inner magnetosphere (DeForest and McIlwain, 1971), causing auroras (Akasofu 1964) in the midnight sector at geomagnetic latitudes of 65° to 70° and slightly lower (the auroras occur both in the
25 northern and southern polar regions). The auroras also spread to all longitudes covering the Earth's magnetosphere at the above latitudes if the storm is intense and long lasting.

The auroras are caused by the influx of energetic ~10 to 100 keV electrons into the outer regions of the magnetosphere (Anderson 1958; Hosokawa et al. 2020) plus precipitation into the ionosphere causing the diffuse auroras and parallel electric fields above the ionosphere accelerating electrons to ~1 to 10 keV causing the discrete auroras (Carlson et al., 1998). The
30 electrons impact atmospheric atoms and molecules at a height of ~110 to 90 km, excite them and decay giving off auroral lines of violet, green and red light. The influx of the energetic electrons also causes the upwelling of oxygen ions to heights where



they will affect the orbiting satellites, causing enhanced drag on the satellites and eventual lowering of their orbits. This is the standard picture of low altitude satellite drag during magnetic storms.

35 Three different scenarios were proposed in 2022 to explain the losses of the Starlink satellites: Tsurutani et al. (2022), Dang et al., (2022), and Fang et al. (2022). Pitout et al. (2022) disagreed and cast doubts that two smallish magnetic storms could have caused the Starlink satellite losses. In 2023, Kakoti et al. (2023) have proposed a new mechanism involving the “combined effects of neutral dynamics and electrodynamic forcing on the dayside ionosphere”. None of the above works have had the information of the individual Starlink satellite orbits. We have obtained NORAD trackings of many of the individual satellites and will present our findings here. These results should be useful for modelers to understand in more detail the
40 satellite loss mechanisms.

2 Starlink Launch

On 2022 February 3, at 18:13 UT, SpaceX launched the rocket Falcon 9 Block 5 with the objective of deploying the satellites for the Starlink Group 4-7, the sixth launch to the Starlink Shell 4. This launch received the international COSPAR identification ID: 2022-010. A video by Manley (2021) illustrates how two stacks of Starlink satellites could be put into orbit
45 from a single launch vehicle. In this example, each stack of ~30 satellites can be released in different directions. When the satellites separate from this stack, they start individual movements, sometimes colliding gently with others before entering into their individual flight orbits. For the February 3 launch, there were 20 satellites in each stack. After the launch, the satellites may be put into edge-on directions with the solar panels parallel to the satellite bodies in an attempt to reduce drag. However, a telecommand is necessary to make them keep the safehold strategy, demanding some time and requiring some minimum
50 antenna pointing.

The SpaceX mission under this study was composed of 49 Starlink satellites that were initially planned to orbit the Earth at ~540 km circular low-Earth orbit (LEO). The initial planned elliptical orbit was 338 km×210 km, at an inclination of 53.22°. Once the initial elliptical orbits were obtained, SpaceX would use onboard propulsion to raise the orbits.

The February 3 deployment of the satellites occurred 15 minutes and 31 seconds after the liftoff, at a release time of 18:28 UT.
55 SpaceX considered the launch successful, since the releasing of the satellites occurred in the expected orbits, the rocket stage was recovered as planned, and all the satellites were able to switch to autonomous flight mode.

3 Space Weather for the Period

From the time of launch until a day after it, the near-Earth space weather conditions were disturbed with the occurrences of two geomagnetic storms. Figure 1 shows the interplanetary and geomagnetic conditions for the period. The solar wind plasma and IMF data at 1 AU are time shifted from the spacecraft location at the L1 libration point ~0.01 AU upstream of the Earth
60 to the nose of the Earth’s bow shock. The IMF components are given in the geocentric solar magnetospheric (GSM) coordinate



system. The solar/interplanetary data were obtained from the NASA's OMNI database (Papitashvili and King, 2020), and the storm-time SYM-H index from the World Data Center for Geomagnetism, Kyoto, Japan (World Data Center for Geomagnetism et al., 2022).

65

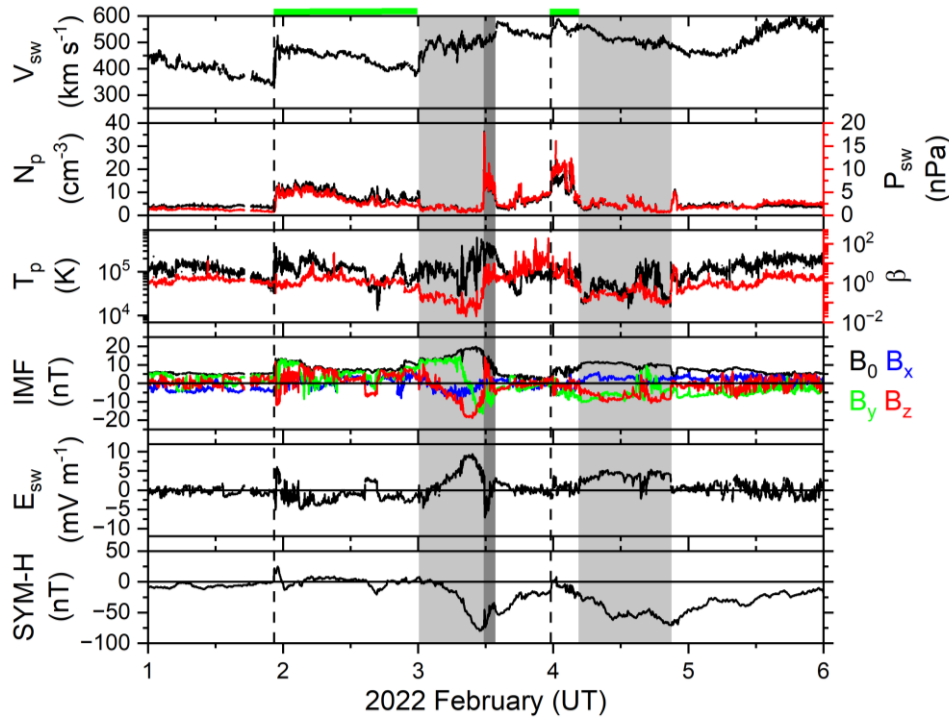


Figure 1: The interplanetary and geomagnetic conditions during 2022 February 1–5. From top to bottom, the panels are: the solar wind speed V_{sw} ; the plasma density N_p (black, legend on the left), and ram pressure P_{sw} (red, legend on the right); temperature T_p (black, legend on the left), and plasma- β (red, legend on the right); the interplanetary magnetic field (IMF) magnitude B_0 (black), and B_x (blue), B_y (green), B_z (red) components; electric field E_{sw} ; and the geomagnetic SYM-H index. The vertical dashed lines indicate interplanetary fast forward shocks. The light gray shadings indicate magnetic clouds (MCs), and the dark gray shading indicates a solar filament propagated to 1 au. Interplanetary sheaths are marked by green bars at the top. The figure is modified from Tsurutani et al. (2022).

70

75 A few days prior to the Starlink satellite launch, on January 29, at ~23:00 UT, an M1.1 solar flare erupted from the active region AR 2936. A coronal mass ejection (CME) was released from this same active region at 23:36 UT. The geomagnetic impact of the interplanetary counter part of the CME or the interplanetary CME (ICME) was the occurrence of a moderate storm (Gonzalez et al. 1994; Echer et al. 2008) with a peak SYM-H intensity of -80 nT on February 3. A second (moderate) geomagnetic storm with a SYM-H intensity of -71 nT occurred on February 4.

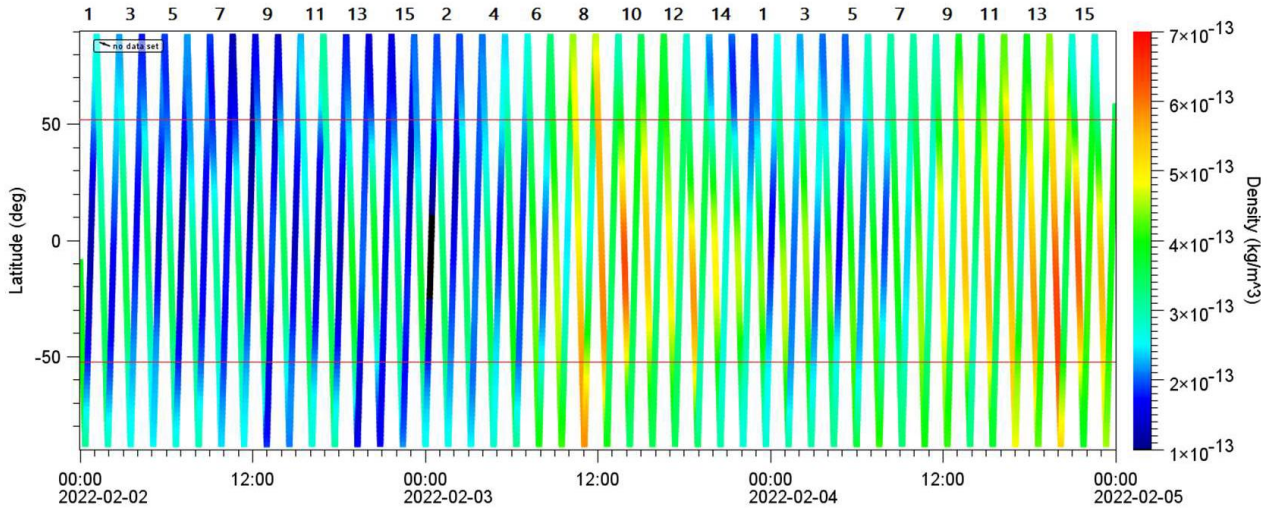
80 The speed of the ICME at 1 au was ~ 500 km s $^{-1}$. This is classified as a moderately fast ICME (faster than the slow solar wind speed of ~ 350 to 400 km s $^{-1}$), thus caused an upstream shock and a sheath. The upstream fast forward shock reached the Earth at $\sim 22:19$ UT on February 1 (indicated by a vertical dashed line). It caused a sudden impulse (SI+) of 22 nT noted in the SYM-



H index. A high-density sheath is present from the shock to the magnetic cloud (MC) portion of the ICME. The sheath following the shock did not contain major southward IMFs, so was generally not geoeffective. The MC portion of the ICME is identified (Burlaga et al. 1981; Tsurutani et al. 1988) by high IMF magnitude BT and low plasma- β (the ratio between the plasma thermal pressure and the magnetic pressure), and is shown by a light gray shading. The MC extends from ~23:54 UT on February 2 to ~13:44 UT on February 3. The IMF Bz component of the MC has the characteristic “fluxrope” configuration with a southward component followed by a northward component. During the southward IMF interval, the SYM-H index decreased to a peak value of -80 nT at ~10:56 UT on February 3. Thus, the magnetic storm is caused by the magnetic reconnection process (Dungey 1961). The dark gray shaded region is the high-density solar filament portion of the ICME (Illing & Hundhausen 1986; Burlaga et al. 1998). The filament causes a compression of the magnetosphere and a sudden increase in the SYM-H index to -39 nT.

A second fast forward shock is identified at ~23:37 UT on February 3 (marked by a vertical dashed line). The shock caused a SI^+ of ~17 nT. The following sheath did not contain any major IMF southward component, so again it was not geoeffective. The MC portion of the second ICME is indicated by a light gray shading from ~04:37 UT to ~21:02 UT on February 4. The MC had a peak IMF BT of ~12 nT at ~08:02 UT. The MC Bz component profile is different from the previous MC. Bz is negative or zero throughout the MC. The negative Bz causes the second magnetic storm of peak intensity -71 nT at ~20:59 UT on February 4. There was no solar filament during this second ICME event. From Fig. 1, it is clear that SpaceX launched their Starlink satellites into a moderate intensity magnetic storm.

The effects of these storms on the atmospheric mass density are analyzed using data from the Swarm B satellite (Fig. 2). The Swarm mission is operated by the European Space Agency. Swarm B is in a circular orbit at ~500 km, with an inclination of ~88° and orbital period of ~90 minutes, so there are about 15 orbits per day. The orbits have been numbered for each day. At 00:00 UT on February 2, the satellite was at ~-10° latitude at ~09:00 local time (LT) on the dayside, and was moving towards the south pole. The mass density is $\sim 3.5 \times 10^{-13}$ kg m⁻³ (a light blue color). Continuing in time as the orbit crosses over the south pole and enters the nightside ionosphere at ~20:00 LT, it is noticed that between -53° and $+53^\circ$ the density reduces to $\sim 1.5 \times 10^{-13}$ kg m⁻³ (a dark blue color). The other orbits on February 2 show a similar pattern between the nightside and dayside passes.



110 **Figure 2: The Swarm B mass impact data for February 2–4. The mass density is shown as a function of UT (x-axis) and geographic latitude (y-axis). It can be noted that the observations cover both day (north-to-south hemispheric passes) and night (south-to-north hemispheric passes) sides of the globe. February 2 was a quiet day before the two magnetic storms and is shown as a “quiet-day reference”. The mass density values are given in linear color scale on the right. Two red horizontal lines at +53° and –53° indicate the upper limits of the intended Starlink satellite orbits. Swarm B orbits on each day from the north pole to the south pole and back are marked by numbers from 1 to 15. Partial orbit 1 for February 2 is shown at the beginning of the figure.**

115

On orbit 8 of February 3, there is the first sign of a change (increase) in the mass impact at middle and low latitudes ($\sim 5.0 \times 10^{-13}$ kg m⁻³, an orange color). This occurs at the south pole crossing at $\sim 10:00$ UT, just before the peak of the first magnetic storm. There is a density enhancement (orange coloration) throughout this downward dayside pass, across the magnetic equator and to the south pole. There is a local maximum of density at $\sim 14:00$ UT and $\sim 09:00$ LT at 10° latitude. On orbits 9–13 of February 3, the predominant density enhancements are on the dayside passes in the equatorial and midlatitude ranges. The enhancements are larger than those at higher latitudes. The maximum density of $\sim 5.5 \times 10^{-13}$ kg m⁻³ occurred at $\sim 19:00$ UT and $\sim 09:00$ LT. This represents a density peak increase of $\sim 50\%$ relative to the quiet daytime density (February 2).

On orbits 9–13 of February 3, the nightside equatorial and midlatitude densities are $\sim 3.5 \times 10^{-13}$ kg m⁻³ (light green color). This is higher than the February 2 (quiet time) nightside densities of $\sim 1.5 \times 10^{-13}$ kg m⁻³. Thus, during the magnetic storm, the nightside peak densities increased by $\sim 100\%$. It is noted that the nighttime peak densities are less than the daytime peak densities. This latter feature will be explained later in this paper.

The high impact mass (orange color) fades out by the end of February 3 and does not start again until orbit 8 of February 4. A density peak of $\sim 5.3 \times 10^{-13}$ kg m⁻³ at the equatorial region on orbit 8 occurred at $\sim 12:00$ UT. This is approximately 10 hours after the slowly developing second magnetic storm started at $\sim 00:15$ UT on February 4. From orbit 8 to 11 the predominant density enhancement occurs at the equatorial to middle latitudes with little or no enhanced impact in the auroral/polar regions. The maximum density of $\sim 6.3 \times 10^{-13}$ kg m⁻³ occurred at $20:00$ UT on dayside pass 14, and extended from $\sim -15^\circ$ to -60°

130



latitudes. The peak time is coincident with the peak in the second magnetic storm. On passes 15 and 16, the density decreases, and the enhanced density occurs mainly at the equator and middle latitudes. The maximum density during this second storm event was ~80% higher than the dayside density values detected on February 2.

135 The nightside density on orbit 14 on February 4 was $\sim 4.3 \times 10^{-13}$ kg m⁻³. This is ~190% higher than the quiet time value on February 2. The nighttime peak densities are lower than the daytime peak densities, similar to the first storm features. The data for February 5 and 6 look similar to the quiet day interval of February 2, so are not shown to conserve space.

4 Magnetic Storm Effects on Starlink Satellite Survivability

Among the 49 released satellites, only 17 could be tracked by the North American Defense Command (NORAD) some days
 140 later. Thirty-two satellites were never listed by NORAD, thus we assume that they were immediately lost after launch. This may have happened due to problems in tracking them (due to extremely fast orbital decays in the first hours after the release or due to substantially different satellite positions than expected for the launch).

Considering the events since the start of the deployment of the Group 4 satellites, in 2021 November, the Starlink launch efficiency have been around 97.5% successful for the last 75 launches to date. However, for the launch being analyzed here,
 145 Starlink Group 4-7, represents a significant reduction in this efficiency, with an orbit insertion failure rate of 77.6%. Table 1 shows the statistics of the launches for the 75 most recent Starlink satellite launches, up to 2023 September. For the calculation of failure percentage, only satellites that failed during the orbit injection process were considered.

150 **Table 1. Statistics on Starlink satellite launches from 2021 November (when Group 4 began to be deployed) to 2023 September 12, with the events ordered according to the launch date. The events marked with “*” indicate launches with another satellite in a rideshare configuration. The Table information was taken from McDowell (2023) and Wikipedia (2022).**

Mission	Launch Number	Launch Date (Year-DOY)	Number of Satellites	Early Deorbit	Failure (%)
Starlink Group 4-1	33	2021-104	53	1	1.9
Starlink Group 4-3	34*	2021-115	48	0	0.0
Starlink Group 4-4	35	2021-125	52	1	1.9
Starlink Group 4-5	36	2022-001	49	0	0.0
Starlink Group 4-6	37	2022-005	49	0	0.0
Starlink Group 4-7	38	2022-010	49	38	77.6
Starlink Group 4-8	39	2022-016	46	0	0.0
Starlink Group 4-11	40	2022-017	50	1	2.0
Starlink Group 4-9	41	2022-022	47	0	0.0
Starlink Group 4-10	42	2022-025	48	0	0.0
Starlink Group 4-12	43	2022-029	53	6	11.3
Starlink Group 4-14	44	2022-041	53	0	0.0
Starlink Group 4-16	45	2022-045	53	0	0.0
Starlink Group 4-17	46	2022-049	53	0	0.0
Starlink Group 4-13	47	2022-051	53	0	0.0
Starlink Group 4-15	48	2022-052	53	0	0.0
Starlink Group 4-18	49	2022-053	53	0	0.0
Starlink Group 4-19	50	2022-062	53	0	0.0
Starlink Group 4-21	51	2022-076	53	1	1.9



Starlink Group 3-1	52	2022-077	46	0	0.0
Starlink Group 4-22	53	2022-083	53	0	0.0
Starlink Group 3-2	54	2022-084	46	0	0.0
Starlink Group 4-25	55	2022-086	53	2	3.8
Starlink Group 4-26	56	2022-097	52	1	1.9
Starlink Group 3-3	57	2022-099	46	0	0.0
Starlink Group 4-27	58	2022-101	53	0	0.0
Starlink Group 4-23	59	2022-104	54	3	5.6
Starlink Group 3-4	60	2022-105	46	0	0.0
Starlink Group 4-20/SLTC	61*	2022-107	51	5	9.8
Starlink Group 4-2/BW3	62*	2022-111	34	3	8.8
Starlink Group 4-34	63	2022-114	54	1	1.9
Starlink Group 4-35	64	2022-119	52	1	1.9
Starlink Group 4-29	65	2022-125	52	0	0.0
Starlink Group 4-36	66	2022-136	54	0	0.0
Starlink Group 4-31	67	2022-141	53	0	0.0
Starlink Group 4-37	68	2022-175	54	0	0.0
Starlink Group 5-1	69	2022-177	54	0	0.0
Starlink Group 2-4	70	2023-010	51	1	2.0
Starlink Group 5-2	71	2023-013	56	1	1.8
Starlink Group 2-6	72*	2023-014	49	1	2.0
Starlink Group 5-3	73	2023-015	53	1	1.9
Starlink Group 5-4	74	2023-020	55	1	1.8
Starlink Group 2-5	75	2023-021	51	1	2.0
Starlink Group 6-1	76	2023-026	21	6	28.6
Starlink Group 2-7	77	2023-028	51	0	0.0
Starlink Group 2-8	78	2023-037	52	0	0.0
Starlink Group 5-5	79	2023-042	56	0	0.0
Starlink Group 5-10	80	2023-046	56	0	0.0
Starlink Group 6-2	81	2023-056	21	1	4.8
Starlink Group 3-5	82	2023-058	46	0	0.0
Starlink Group 5-6	83	2023-061	56	0	0.0
Starlink Group 2-9	84	2023-064	51	0	0.0
Starlink Group 5-9	85	2023-065	56	1	1.8
Starlink Group 6-3	86	2023-067	22	1	4.5
Starlink Group 2-10	87	2023-078	52	0	0.0
Starlink Group 6-4	88	2023-079	22	3	13.6
Starlink Group 5-11	89	2023-083	52	0	0.0
Starlink Group 5-7	90	2023-088	47	0	0.0
Starlink Group 5-12	91	2023-090	56	0	0.0
Starlink Group 5-13	92	2023-094	48	0	0.0
Starlink Group 6-5	93	2023-096	22	0	0.0
Starlink Group 5-15	94	2023-099	54	0	0.0
Starlink Group 6-15	95	2023-102	15	0	0.0
Starlink Group 6-6	96	2023-105	22	0	0.0
Starlink Group 6-7	97	2023-107	22	1	4.5
Starlink Group 6-8	98	2023-113	22	0	0.0
Starlink Group 6-20	99	2023-115	15	0	0.0
Starlink Group 6-9	100	2023-119	22	1	4.5
Starlink Group 6-10	101	2023-122	22	0	0.0
Starlink Group 7-1	102	2023-124	21	0	0.0
Starlink Group 6-11	103	2023-129	22	0	0.0
Starlink Group 6-13	104	2023-131	22	0	0.0
Starlink Group 6-12	105	2023-134	21	0	0.0
Starlink Group 6-14	106	2023-138	22	0	0.0
Starlink Group 7-2	107	2023-141	21	0	0.0



On February 5, a first group of 6 Starlink satellite trackings were made available by NORAD. All these satellites had very low perigees, ~200 km altitude. The apogees were also very low, always below 350 km, and in some cases as low as 250 km. For the latter satellites, the apogees were not far from the perigee altitudes. Since the orbit injection velocities were too low for such unexpected low orbits, these satellites did not survive long. Some of these remaining 6 were also lost after a few tracking. A second group of satellites, formed by 11 satellites, was tracked some days later, on February 8. These satellites were able to perform their ascending movements, changing from elliptical to circular orbits, and rising to higher and more stable intermediate orbits at ~350 km. The satellites were kept in this position for a few days. Afterwards their orbits were boosted to their final altitudes of ~540 km. However, one of these satellites, Starlink #3165, showed communication problems beginning on 2022 October 31. Although it is still being tracked in flight, it is currently out of control and deorbiting. The cause of this communication failure is still undisclosed, and thus it is not possible to verify whether it could be related to the problems experienced during the first hours/days after launch.

5 Satellite Tracking Timeline

In order to make it easier to understand all the sequence of events, a timeline was created with the space weather events, individual satellite tracking and other available information. Figure 3 shows this timeline. The satellites are identified by their NORAD numbers. Only those tracked after February 8 were linked to their Starlink numbers.

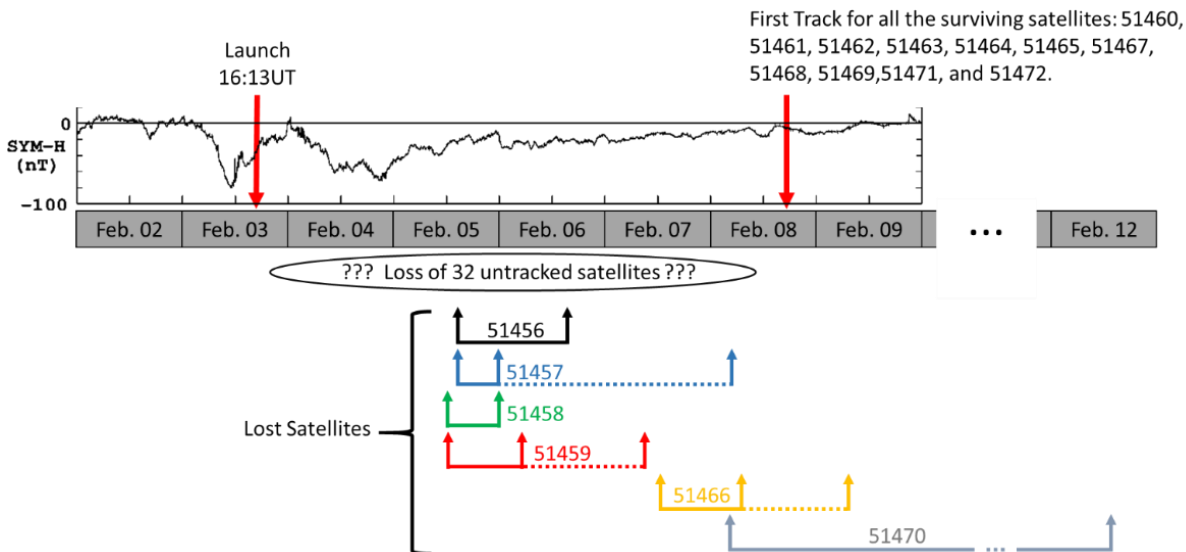


Figure 3: Timeline for the satellite tracking occurring between February 2 and 12, 2022.



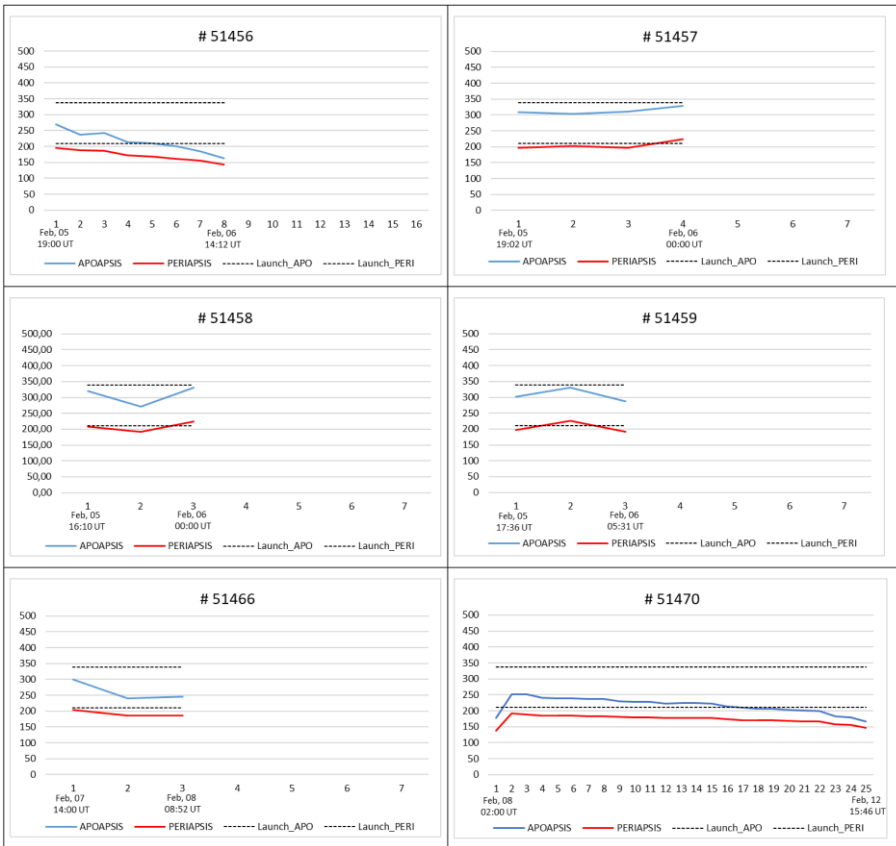
Figure 3 shows a plot of the SYM-H index which indicates the geomagnetic disturbances and the occurrence of geomagnetic storms. The two storm peaks are: SYM-H = -80 nT on February 3 and SYM-H = -71 nT on February 4. The red downward pointing arrows indicate the launch times, and the beginning of the tracking of the 11 surviving satellites, respectively. It should be noted that the Starlink satellites were launched in the recovery phase of the first storm (SYM-H increasing from its minimum value). Thus, the satellites are expected to have experienced effects from the first magnetic storm. It is also noticed that the second storm main phase started at the beginning of February 4 and continued for almost the entire day. Any Starlink satellites surviving the first storm would experience the effects of the second storm as well.

At the bottom of Fig. 3, the upward arrows indicate the beginning and end times of the tracking for all other lost satellites (besides the original 32 satellites never tracked). For satellites 51457, 51459, and 51466, the extended dashed line and another arrow indicate the “official” decay times. An oval mark indicates the time interval when the 32 satellites were expected to be tracked, but were already lost.

6 Surviving Satellite Orbits Information

Figures 4 and 5 show the orbit information for the decayed satellites and for the operational satellites, respectively.

In Fig. 4 the vertical axes give the satellite altitudes and the horizontal axes give the tracking sequences. The two dashed black lines indicates the perigees and the apogees expected for the satellite launches, 210 km and 338 km, respectively. The red and blue lines indicate the apogee and perigee at each tracking point. The date and time of the first and last tracking is indicated under the horizontal axis.



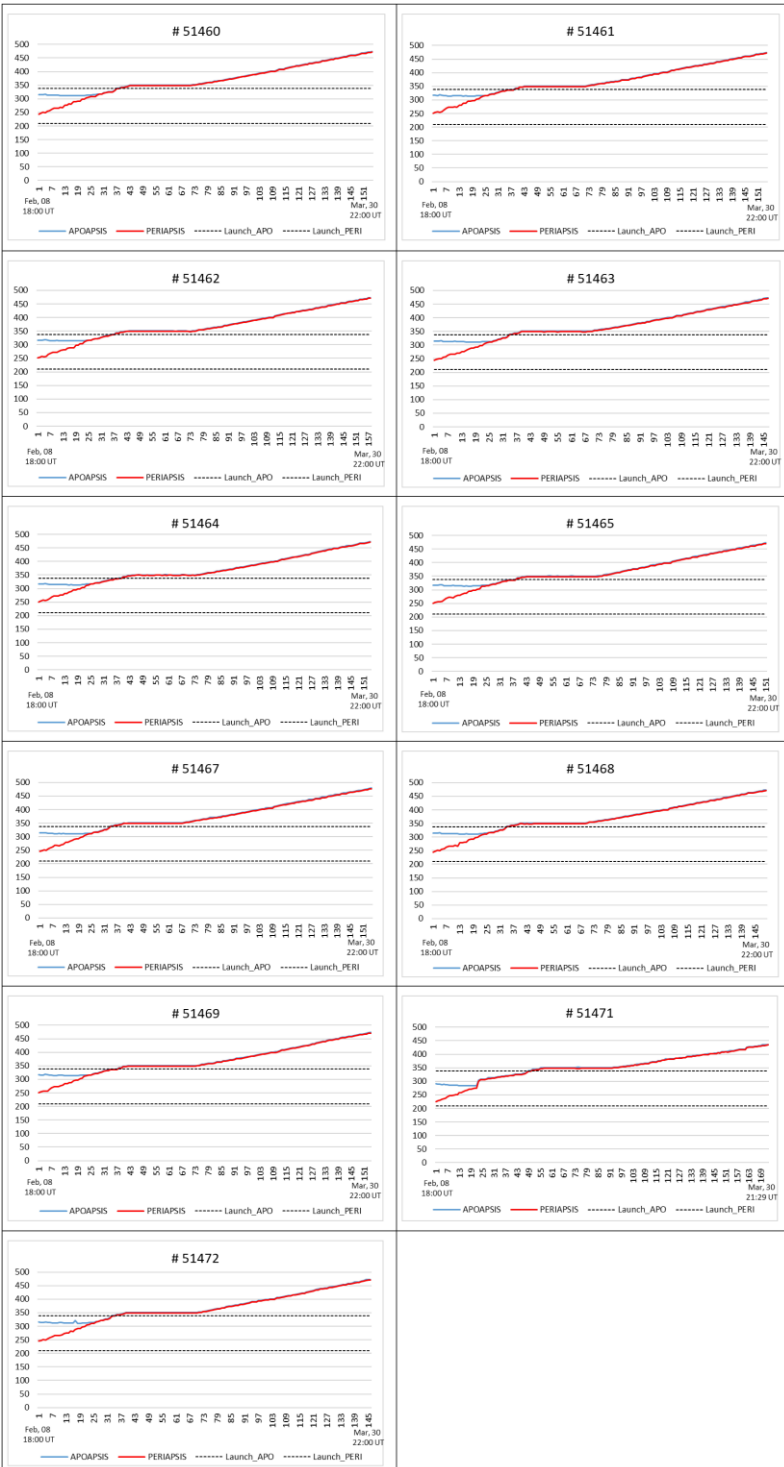
190 **Figure 4:** Panels showing the orbit perigees (red lines) and apogees (blue lines) for each of the decayed satellites. The vertical axis in each panel gives the satellite height, and the horizontal axis indicates the tracking sequence. The dates and times under the horizontal axis indicates the time of the first and the last tracking. The two dashed black lines indicate the perigees and the apogees for the launch.

195 For all the above cases, the satellites were in very low orbits in the first track, close to the lowest orbits expected for the lowest perigees. The apogees were always very far (lower) from the expected values for the launch, and sometimes even closer to the values expected for perigees.

It can be noted that some satellites started to rise in altitude, but most likely were lost due to insufficient thrust in such low orbits with increased atmospheric drag.

200 A contrasting scenario is shown in Fig. 5. All of these satellites survived the launching episode. After initial tracking by NORAD (all of them starting on 2022 February 8) they were boosted by onboard propulsion to safer (higher) altitudes.

The plots are in the same format as in Fig. 4, but the horizontal axes now indicate the initial tracking (on February 8) until March 30.



205

Figure 5: Panels showing the orbit perigees (red lines) and apogees (blue lines) for the surviving satellites. The vertical axes give the satellite altitudes, and the horizontal axes indicate the tracking sequences from 2022 February 8 to March 30. The two dashed black lines indicate the perigees and apogees expected at the time of the launch.



210 It is interesting to note from Fig. 5 that all of the satellites started their orbits in elliptical configurations, with apogee and perigee values much higher than the (decayed) satellites shown in Fig. 4. The Fig. 5 satellite orbits were very close to the specified values for the launch.

The orbit shapes changed to circular configurations (indicated by the merging of the red and blue lines) with subsequent altitude increases to intermediate orbital configurations. The rising to the final orbits were done very slowly, and none of the satellites had reached the final ~540 km altitude originally envisioned by March 30, almost two months after the launch.

215 **7 Discussion and Conclusions**

We have shown the available SpaceX Starlink satellite orbital plots as well as the sequence of events observed. The NORAD system was never able to identify 32 satellites. They were presumably lost between a few hours to days after launch. This implies possible quite heavy drag in the equatorial to midlatitude (up to 53° latitude) regions of the atmosphere at ~200 km altitudes. This will be a priority to investigate the physics and causes of this effect during magnetic storms.

220 Some of the satellites did survived the dual storm event. Since all the Starlink satellites were launched at the same time and at the same altitude, and they had such widely varying fates (some being immediately lost, some surviving) it is clear that each one had a different response to the magnetic storm density effects and/or had strong collisions with other satellites.

225 It took several more days for NORAD to make available the tracking of another train of 11 other satellites. The latter satellites were in more favorable positions (altitudes), allowing their recovery and rise to more stable orbits.

One can note from the above discussion that different satellites had extremely different orbital decay rates, indicating that one scenario can not fit all 43 satellite cases. In particular, we are most concerned about the possible losses of 32 of the satellites within the first 48 hours of launch such that they could never be tracked by NORAD.

8 Comments on Previous Explanations of Starlink Satellite Losses

230 Before it was known that the Starlink satellites never reach their intended ~500 km altitude, Tsurutani et al. (2022) proposed that prompt penetrating electric fields (PPEFs; Tsurutani et al. 2004, 2007; Lakhina & Tsurutani 2017) could be responsible for those losses. Their Fig. 2 (reshown here as Fig. 2) demonstrated that dayside near-equatorial density increases occurred at 500 km altitude during the two magnetic storms. However, the present orbital analyses indicate that none of the satellites lost on the first two days reached altitudes higher than 200 km for the entire orbit (they were still in elliptic trajectories). Thus, this loss mechanism must be discarded for the Starlink cases. However, on a positive note, it was shown for the first time using the Swarm satellite deceleration data that storm time PPEFs may be a main loss mechanism for satellites orbiting at ~400 to 500 km altitudes.



On the other hand, the Dang et al. (2022) scenario does not explain completely such losses in so low latitudes. They used a global upper atmospheric model (TIEGCM) to estimate the Joule heating by Ohmic dissipation at ionospheric altitudes. However, the Joule heating proposed by the authors was more remarkable in high latitudes, while the increases observed in latitudes below 53° were too small to create such an effect. Dang et al. predicted losses in 5 to 7 days assuming a constant 210 km satellite altitude. This cannot explain the possible immediate losses of the 32 satellites.

Fang et al. (2022) have used numerical simulations to show 50-125% neutral density enhancements between 200 and 400 km. Their argument based on effects of Joule heating produced in high latitudes propagating to lower latitudes by large-scale gravity waves, with phase speeds of 500 to 800 m s⁻¹ (Fuller-Rowell et al. 2008). This propagation may take from 3 to 4 hours and are in addition to the effects of increased UV and EUV fluxes due to the flares. Previous events had taken up to 30 hours to the atmosphere returns to the undisturbed condition. We note, however, that Fig. 2 in the present work showed that there were very low Joule heating effects in the auroral zone during both of these magnetic storms, thus negating the high latitude Joule heating effects assumed in the model.

Kakoti et al. (2023) have suggested that “significant morning-noon electron density reductions elucidated storm-induced equatorward thermospheric wind which caused the strong morning counter electrojet by generating the disturbance dynamo electric field. Sub-storm related magnetospheric convection resulted in significant noon-time peak in equatorial electrojet on 4 February”. This is a very interesting result. We wonder whether it can explain the near-immediate loss of 32 of the Starlink satellites?

9 Final Comments

The losses of the February 2022 Starlink satellites were quite varied. Different satellites came down at different times. Some even survived. Clearly a simple statement of a value of enhanced drag is insufficient to explain the enormous variability in the different satellite responses. The most difficult problem is explaining the loss of 32 satellites within the first 2 days after launch. At this time we do not have a physical explanation that involves the two magnetic storms. We hope to stimulate the scientific community to search for currently unknown physical mechanisms that might be able to explain such enormous drag occurring near equatorial regions at low altitudes.

It is also a remote possibility that the immediate 32 satellite losses were due to satellite-satellite collisions instead of or precipitated by increased drag during the magnetic storms.

Competing interests

One of the co-authors is a member of the editorial board of Nonlinear Processes in Geophysics.



Acknowledgments

The work of R.H. is funded by the Chinese Academy of Sciences “Hundred Talents Program”. E.E. thanks Brazilian CNPq for research grant (contract PQ-301883/2019-0).

Data Availability Statement

270 The solar/interplanetary data were obtained from the NASA’s OMNI database (Papitashvili and King, 2020), and the storm-time SYM-H index from the World Data Center for Geomagnetism (World Data Center for Geomagnetism et al., 2022). The Swarm data were obtained from Swarm (2022). Starlink satellite launches information is accessible at Wikipedia (2022) and McDowell (2023).

References

- 275 Akasofu, S. I.: The development of the auroral substorm. *Planetary and Space Science*, 12, 273-282. [https://doi.org/10.1016/0032-0633\(64\)90151-5](https://doi.org/10.1016/0032-0633(64)90151-5), 1964.
- Anderson, K. A.: Soft radiation events at high altitude during the magnetic storm of August 29-30, 1957. *Phys. Rev.* 111, 1397-1405. <https://doi.org/10.1103/PhysRev.111.1397>, 1958.
- BBC News.: SpaceX loses 40 satellites to geomagnetic storm a day after launch. BBC News. Published on 2022 February 9.
- 280 <https://www.bbc.com/news/world-60317806>, 2022.
- Burlaga, L., Sittler, E., Mariani, F., and Schwenn, R.: Magnetic loop behind an interplanetary shock: Voyager, Helios, and IMP 8 observations. *J. Geophys. Res.* 86, 6673-6684. <https://doi.org/10.1029/JA086iA08p06673>, 1981.
- Carlson, C. W., McFadden, J. P., Ergun, R. E., Temerin, M., Peria, W., Mozer, F. S., Klumpar, D. M., Shelley, E. G., Peterson, W. K., Moebius, E., Elphic, R., Strangeway, R., Cattell, C., and Pfaff, R.: FAST observations in the downward auroral current
- 285 region: Energetic upgoing electron beams, parallel potential drops, and ion heating. *Geophys. Res. Lett.* 25, 2017-2020. <https://doi.org/10.1029/98GL00851>, 1998.
- Clark, S.: Solar storm dooms up to 40 new Starlink satellites. *SpaceFlight Now*. Published on February 08, 2022. <https://spaceflightnow.com/2022/02/08/solar-storm-dooms-40-new-starlink-satellites>, 2022.
- Dang, T., Li, X., Luo, B., Li, R., Zhang, B., Pham, K., Ren, D., Chen, X., Lei, J., and Wang, Y.: Unveiling the space weather
- 290 during the Starlink Satellites destruction event on 4 February 2022. *Spa. Weath.*, 20, e2022SW003152. <https://doi.org/10.1029/2022SW003152>, 2022.
- DeForest, S.E. and McIlwain, C. E.: Plasma clouds in the magnetosphere, *J. Geophys. Res.*, 76, 16, 3587-3611.
- Dungey, J. W. (1961). Interplanetary magnetic field and the auroral zones. *Phys. Rev. Lett.* 6, 47-48. <https://doi.org/10.1103/PhysRevLett.6.47>, 1971.



- 295 Fang, T.-W., Kubaryk, A., Goldstein, D., Li, Z., Fuller-Rowell, T., Millward, G., Singer, H. J., Steenburgh, R., Westerman, S., and Babcock, E.: Space weather environment during the SpaceX Starlink satellite loss in February 2022. *Space Weather*, 20, e2022SW003193. <https://doi.org/10.1029/2022SW003193>, 2022.
- Fuller-Rowell, T. J., R. Akmaev, F. Wu, A. Anghel, N. Maruyama, D. N. Anderson, M. V. Codrescu, M. Iredell, S. Moorthi, H.-M. Juang, Y.-T. Hou, and Millward, G.: Impact of terrestrial weather on the upper atmosphere. *Geophys. Res. Lett.*, 35, L09808. <https://doi.org/10.1029/2007GL032911>, 2008.
- 300 Gonzalez, W. D., Joselyn, J. A., Kamide, Y., Kroehl, H. W., Rostoker, G., Tsurutani, B. T., and Vasylunas, V. M.: What is a geomagnetic storm? *J. Geophys. Res.* 99, 5571-5792. <https://doi.org/10.1029/93JA02867>, 1994.
- Hosokawa, K., Kullen, A., Milan, S., Reidy, J., Zou, Y., Frey, H. U., Maggiolo, R., and Fear, R.: Aurora in the Polar Cap: A Review. *Space Sci. Rev.* 216, 15. <https://doi.org/10.1007/s11214-020-0637-3>, 2020.
- 305 Illing, R. M. E., and Hundhausen, A. J.: Disruption of a coronal streamer by an eruptive prominence and coronal mass ejection. *Journal of Geophysical Research*, 91. 10951pp. <https://doi.org/10.1029/ja091ia10p10951>, 1986.
- Kakoti, G., Bagiya, M.S., Laskar, F. I., and Lin, D.: Unveiling the combined effects of neutral dynamics and electrodynamic forcing on dayside ionosphere during the 3-4 February 2022 “SpaceX” geomagnetic storms, *Nature Sci. Repts.*, 13:18932. <https://doi.org/10.1038/s41598-023-45900-y>, 2023.
- 310 Lakhina, G. S., and Tsurutani, B. T.: Satellite drag effects due to uplifted oxygen neutrals during super magnetic storms. *Nonl. Proc. Geophys.*, 24, 745-750. <https://doi.org/10.5194/npg-24-745-2017>, 2017.
- Manley, S.: How Do Starlink Satellites Navigate To Their Final Operational Orbits. <https://www.youtube.com/watch?v=VIOr1UyhwWk>, 2021.
- McDowell, J.: Jonathan's Space Pages. [Accessed in 2023 Sep 12]. Available from: <https://planet4589.org>, 2023.
- 315 Papitashvili, Natalia E. and King, Joseph H.: "OMNI 1-min Data" [Data set], NASA Space Physics Data Facility, <https://doi.org/10.48322/45bb-8792>, 2020,
- Paschmann, G., Sonnerup, B. U. Ö., Papamastorakis, I., Sckopke, N., Haerendel, G., Bame, S. J., Asbridge, J. R., Gosling, J. T., Russell, C. T., and Elphic, R. C.: Plasma acceleration at the Earth's magnetopause: evidence for reconnection. *Nature*, 282, 243-246. <https://doi.org/10.1038/282243a0>, 1979.
- 320 Pitout, F., Astafyeva, E., Fleury, R., Maletckii, B., and He J.: Soc. Fran. D'Astrophys. (SF2A). J. Richard et al. editors, 2023.
- SpaceX: Geomagnetic storm and recently deployed Starlink satellites. SpaceX website. Published on February 09, 2022. <https://www.spacex.com/updates/>, 2022.
- Tsurutani, B. T., and Meng, C.-I.: Interplanetary magnetic-field variations and substorm activity. *J. Geophys. Res.*, 77, 2964. <https://doi.org/10.1029/JA077i016p02964>, 1972.
- 325 Tsurutani, B. T., Gonzalez, W. D., Tang, F., Akasofu, S. I., and Smith, E. J.: Origin of interplanetary southward magnetic fields responsible for major magnetic storms near solar maximum (1978-1979). *J. Geophys. Res.* 93, 8519-8531. <https://doi.org/10.1029/JA093iA08p08519>, 1988.



- 330 Tsurutani, B. T., Mannucci, A. J., Iijima, B., Abdu, M. A., Sobral, J. H. A., Gonzalez, W. D., Guarnieri, F., Tsuda, T., Saito, A., Yumoto, K., Fejer, B., Fuller-Rowell, T. J., Kozyra, J., Foster, J. C., Coster, A., and Vasyliunas, V. M.: Global dayside ionospheric uplift and enhancement associated with interplanetary electric fields. *J. Geophys. Res.* 109, A08302. <https://doi.org/10.1029/2003JA010342>, 2004.
- 335 Tsurutani, B. T., Judge, D. L., Guarnieri, F. L., Gangopadhyay, P., Jones, A. R., Nuttall, J., Zambon, G. A., Didkovsky, L., Mannucci, A. J., Iijima, B., Meier, R. R., Immel, T. J., Woods, T. N., Prasad, S., Floyd, L., Huba, J., Solomon, S. C., Straus, P., and Viereck, R.: The October 28, 2003 extreme EUV solar flare and resultant extreme ionospheric effects: Comparison to other Halloween events and the Bastille Day event. *Geophys. Res. Lett.*, 32, L03S09. <https://doi.org/10.1029/2004GL021475>, 2005.
- Tsurutani, B. T., Verkhoglyadova, O. P., Mannucci, A. J., Araki, T., Saito, A., Tsuda, T., and Yumoto, K.: Oxygen ion uplift and satellite drag effects during the 30 October 2003 daytime superfountain event. *Ann. Geophys.* 25, 569-574. <https://doi.org/10.5194/angeo-25-569-2007>, 2007.
- 340 Tsurutani, B. T., Green, J., and Hajra, R.: The Possible Cause of the 40 SpaceX Starlink Satellite Losses in February 2022: Prompt Penetrating Electric Fields and the Dayside Equatorial and Midlatitude Ionospheric Convective Uplift. arXiv:2210.07902 [physics.space-ph], <https://doi.org/10.48550/arXiv.2210.07902>, 2022.
- von Humboldt, A.: Die vollständigste aller bisherigen Beobachtungen über den Einfluss des Nordlichts auf die Magnetnadel angestellt. *AnPh*, 29, 425. <https://doi.org/10.1002/andp.18080290806>, 1808.
- 345 Wikipedia contributors: List of Starlink and Starshield launches [Internet]. Wikipedia, The Free Encyclopedia. [Accessed in 2022 Oct 28]. Available from: https://en.wikipedia.org/w/index.php?title=List_of_Starlink_and_Starshield_launches&oldid=1148257453, 2022.
- World Data Center for Geomagnetism, Kyoto, <https://wdc.kugi.kyoto-u.ac.jp/>. Accessed on October, 2022.